

## 2. Gravitational lenses

### 6. GL MODELS; 6.1. Axially symmetric lens models:

$$P = \rho \frac{kT}{m} \quad , \quad (6.15)$$

$$m\sigma^2 = kT \quad , \quad (6.16)$$

$$\frac{dP}{dr} = -G \frac{M(r)\rho}{r^2} \quad , \quad (6.17)$$

$$\frac{dM(r)}{dr} = 4\pi r^2 \rho \quad , \quad (6.18)$$

$$\rho(r) = \frac{\sigma^2}{2\pi G r^2} \quad , \quad (6.19)$$

$$v_{\text{rot}}^2(r) = G \frac{M(r)}{r} = 2\sigma^2 = C^{\text{te}} \quad , \quad (6.20)$$

$$\Sigma(\xi) = \frac{\sigma^2}{2G\xi} \quad . \quad (6.21)$$

## 2. Gravitational Lenses: 6. GRAVITATIONAL LENS MODELS:

### 6.1. Axially symmetric lens models; 6.1.3. The SIS lens model:

A simple model for the mass distribution in galaxies assumes that the stars and other mass components behave like particles of an ideal gas, confined by their combined, spherically symmetric gravitational lens potential. The equation of state of the 'particles', henceforth called stars for simplicity, takes the form (Narayan and Bartelmann 1997)

$$P = \rho kT / m \quad , \quad (6.15)$$

where  $\rho$  and  $m$  are the mass density and the mass of the stars. In thermal equilibrium, the temperature  $T$  is related to the one-component (observable) velocity dispersion  $\sigma$  of the stars in the galaxy through

$$m\sigma^2 = kT \quad . \quad (6.16)$$

The temperature, or equivalently the velocity dispersion, could in general depend on radius  $r$ , but it is usually assumed that the stellar gas is isothermal, so that  $\sigma$  is constant across the galaxy. The equation of hydrostatic equilibrium then gives

$$\text{with } \frac{dP}{dr} = -G \frac{M(r)\rho}{r^2} \quad , \quad (6.17)$$

$$\frac{dM(r)}{dr} = 4\pi r^2 \rho \quad , \quad (6.18)$$

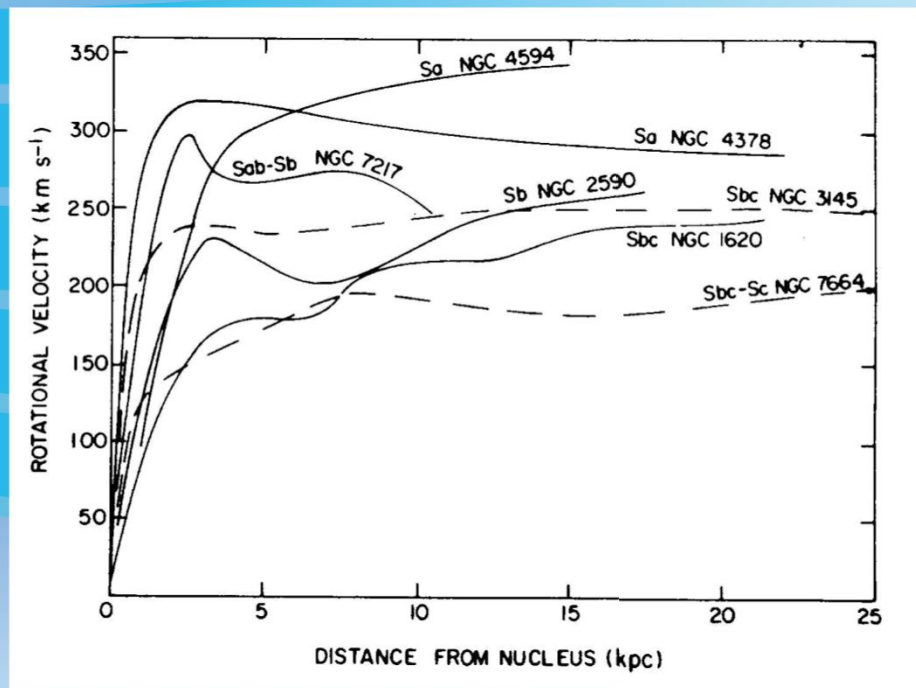
where  $M(r)$  is the mass interior to radius  $r$ . A particularly simple solution of the previous equations is

$$\rho(r) = \frac{\sigma^2}{2\pi G r^2} \quad (6.19)$$

This mass distribution is called the *singular isothermal sphere*.

## 2. Gravitational lenses

### 6. GL MODELS; 6.1. Axially symmetric lens models:



Rotation curves observed for spiral galaxies (Rubin et al. 1978)

### 2. Gravitational Lenses: 6. GRAVITATIONAL LENS MODELS:

#### 6.1. Axially symmetric lens models; 6.1.3. The SIS lens model:

Since  $\rho(r) \propto r^{-2}$ , the mass  $M(r)$  increases  $\propto r$ , and therefore the rotational velocity of test particles in circular orbits in the gravitational potential is

$$v_{\text{rot}}^2(r) = G \frac{M(r)}{r} = 2\sigma^2 = C^{\text{te}} \quad (6.20)$$

The flat rotation curves of galaxies are thus naturally reproduced by this model (see the above figure). [This form of the density law could also have been retrieved assuming that the gradient of the Newtonian potential is  $dU/dr = v^2/r$  and by straight application of the Poisson equation in spherical coordinates, we find that  $\rho(r) = v^2/4\pi Gr^2$ ].

## 2. Gravitational lenses

### 6. GL MODELS; 6.1. Axially symmetric lens models:

$$\underline{\alpha}(\xi) = \underline{\alpha}_0 = 4 \pi \sigma^2 / c^2, \quad (6.22)$$

$$\theta_{A,B} = \theta_s \pm \alpha_0, \quad (6.23)$$

$$\theta_E = \alpha_0, \quad (6.24)$$

$$\mu_E = 4 \theta_E / d\theta_s. \quad (6.25)$$

$$\mu_A = 1 + (\theta_E / \theta_s), \quad (6.26a)$$

$$\mu_B = 1 - (\theta_E / \theta_s). \quad (6.26b)$$

$$\mu_T = \mu_A - \mu_B = 2 \theta_E / \theta_s. \quad (6.27)$$

$$\mu_A = 1 + (\theta_E / \theta_s). \quad (6.28)$$

### 2. Gravitational Lenses: 6. GRAVITATIONAL LENS MODELS:

#### 6.1. Axially symmetric lens models; 6.1.3. The SIS lens model:

Upon projecting the mass of the spherical model with volume density  $\rho(r)$  along the line-of-sight, we easily obtain the expression of the surface mass density  $\left( \Sigma(\xi) = \int \rho(r = \sqrt{\xi^2 + s^2}) ds \right)$

$$\Sigma(\xi) = \frac{\sigma^2}{2G\xi} \quad (6.21)$$

where  $\xi$  is the distance from the center of the two-dimensional profile. Referring to Eq. (4.5) and since  $M(\xi) = 2\pi \int \Sigma(\xi') \xi' d\xi'$ , we obtain the expression of the deflection angle

$$\underline{\alpha}(\xi) = \underline{\alpha}_0 = 4 \pi \sigma^2 / c^2, \quad (6.22)$$

see the corresponding ray tracing and bending angle diagrams.

For  $|\theta_s| \leq \alpha_0 = \underline{\alpha}_0 (D_{ds} / D_{os})$ , the solutions of the one-dimensional SIS lens equation are then  $\theta_{A,B} = \theta_s \pm \alpha_0$ , (6.23)

in accordance with Eq. (4.3). From these equations, we may directly infer that an observer located on the symmetry axis (i.e. for  $\theta_s = 0$ ; see  $O_1$  in the ray tracing diagram) will also see in this case an Einstein ring, the latter one being characterized by the angular radius

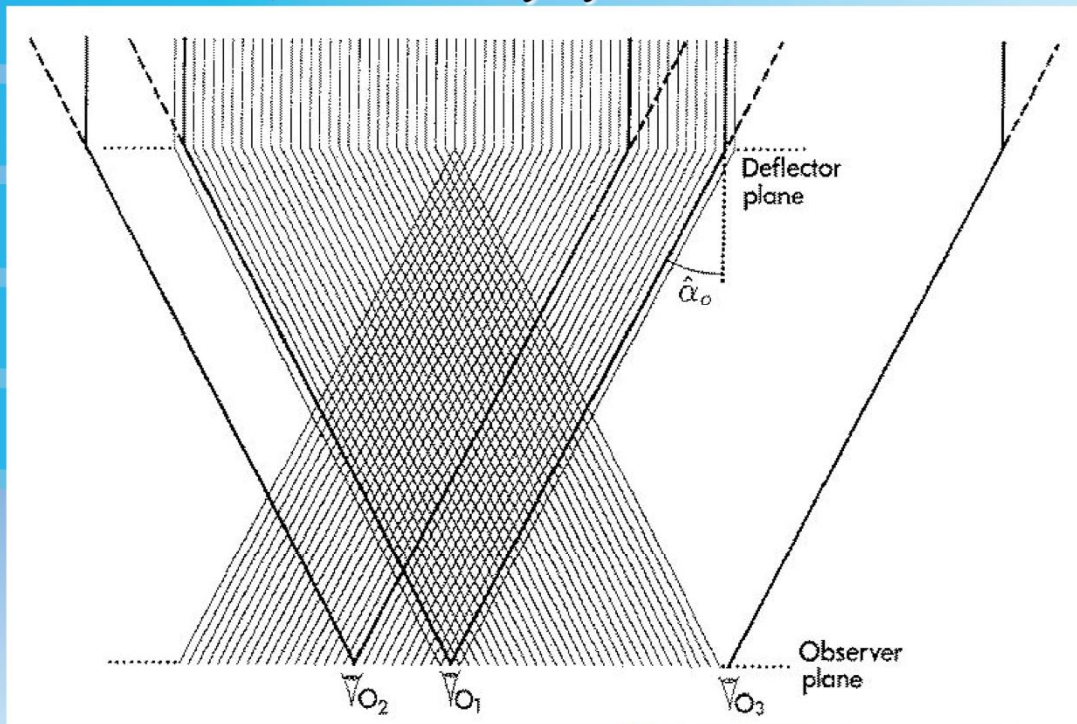
$$\theta_E = \alpha_0, \quad (6.24)$$

and that the magnification of this ring amounts to

$$\mu_E = 4 \theta_E / d\theta_s. \quad (6.25)$$

## 2. Gravitational lenses

### 6. GL MODELS; 6.1. Axially symmetric lens models:



Ray tracing diagram for the SIS lens model.

### 2. Gravitational Lenses: 6. GRAVITATIONAL LENS MODELS:

#### 6.1. Axially symmetric lens models; 6.1.3. The SIS lens model:

This last value for the magnification is found to be twice as large as that for the point mass lens; the reason being that the angular thickness of the SIS Einstein ring is  $2 d\theta_s$  (see the combined bending angle diagram), i.e. it is twice as large as that in the point mass case.

As the observer moves away from the symmetry axis (cf.  $O_2$  in the ray tracing diagram), the Einstein ring also here breaks up in two images with an angular separation  $\Delta\theta = 2\theta_E$  (see the combined bending angle diagram). As long as  $\theta_s \leq \theta_E$ , we easily find by means of Eqs. (4.6) and (6.23) that the (positive and negative) magnification of the two images is

$$\mu_A = 1 + (\theta_E / \theta_s), \quad (6.26a)$$

and

$$\mu_B = 1 - (\theta_E / \theta_s). \quad (6.26b)$$

The net total magnification affecting the two images is thus

$$\mu_T = \mu_A - \mu_B = 2\theta_E / \theta_s. \quad (6.27)$$

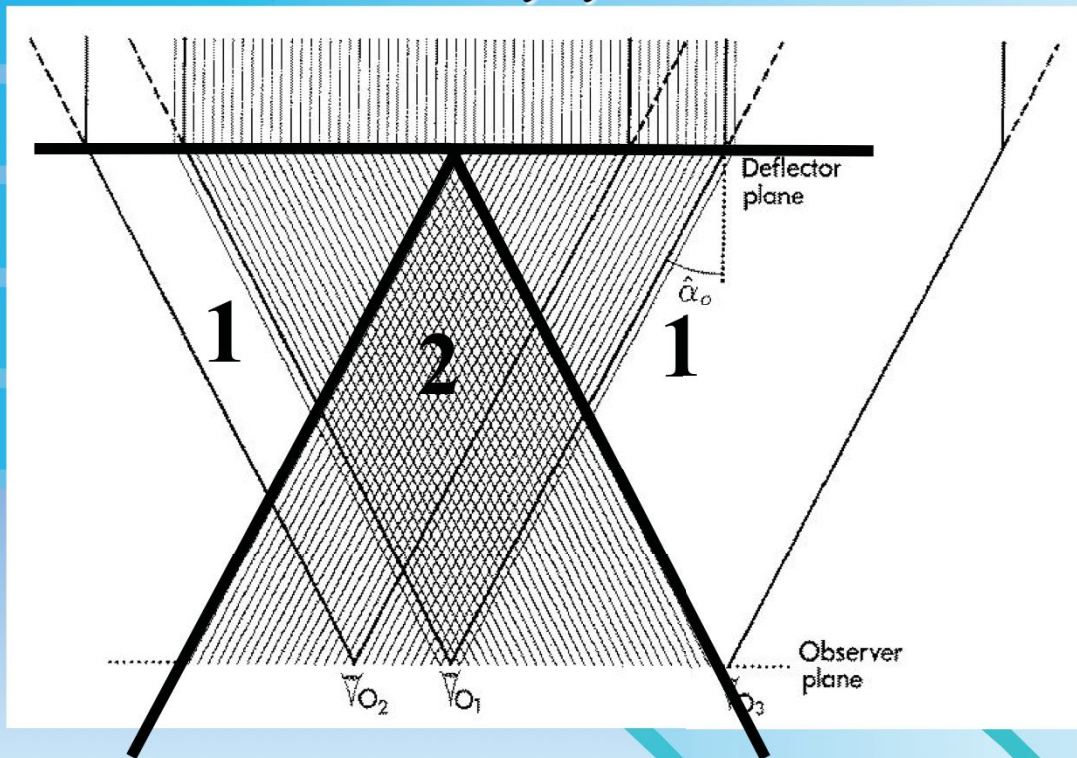
For  $\theta_s > \theta_E$ , the observer only sees one image (cf.  $O_3$  in the ray tracing and combined bending angle diagrams) and its magnification is given by

$$\mu_A = 1 + (\theta_E / \theta_s). \quad (6.28)$$

We see that  $\mu_A \rightarrow 1$  when  $\theta_s$  increases to large values. We recall that the SIS lens model constitutes a good first approximation to simulate the lensing properties of real galaxies over a large range of impact parameters and that it is therefore often being used for estimating lensing probabilities (see section 7). The most serious shortcoming of this model is its too

## 2. Gravitational lenses

### 6. GL MODELS; 6.1. Axially symmetric lens models:



Ray tracing diagram for the SIS lens model.

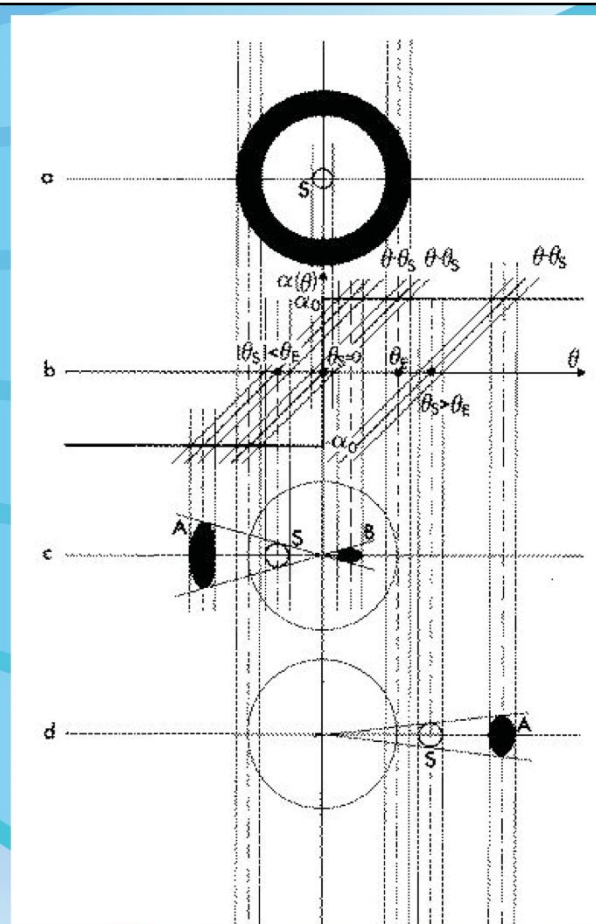
### 2. Gravitational Lenses: 6. GRAVITATIONAL LENS MODELS:

## 2. Gravitational lenses

### 6. GL MODELS:

#### 6.1. Axially symmetric lens models:

Combined bending angle diagram (b) and resulting lensed images produced for the circular source  $S$  by a SIS lens model (a, c and d; see text).



### 2. Gravitational Lenses; 6. GRAVITATIONAL LENS MODELS:

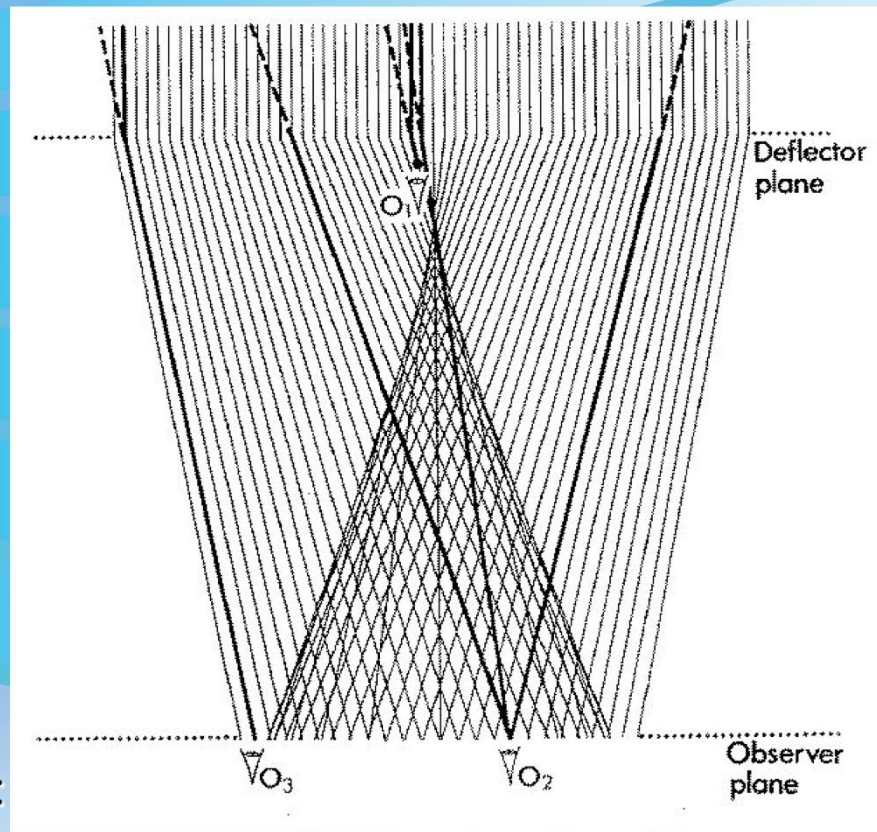
#### 6.1. Axially symmetric lens models; 6.1.3. The SIS lens model:

large deflection for light rays passing near to the center of the galaxy. However, for statistical purposes, this is not too serious since small values of the impact parameter  $\xi$  do occur very seldomly. Since for real (finite) galaxies, the deflection angle obviously tends to zero as the impact parameter gets large, one may naturally introduce truncated singular isothermal sphere models or even more complex ones, as shown in the next section.

## 2. Gravitational lenses

### 6. GL MODELS:

#### 6.1. Axially symmetric lens models:



Ray tracing diagram for the spiral galaxy lens model.

### 2. Gravitational Lenses:

#### 6. GRAVITATIONAL LENS MODELS:

##### 6.1. Axially symmetric lens models:

6.1.4. The spiral galaxy lens model: If we combine Eq. (4.5) with Eq.(5.10) that characterizes the mass distribution of the disk of a spiral galaxy, seen face on, we may easily construct the resulting ray tracing diagram (cf. the above figure) and the combined bending angle diagrams (see next figures) in order to understand the formation of multiple lensed images due to this somewhat more complex deflector model. From these diagrams, we directly see that whenever the observer is located between the lens and the focal point caused by the inner part of the disk (cf.  $O_1$  in the corresponding figures), we have  $\Sigma_0 < \Sigma_c$ , where  $\Sigma_c$  represents the critical surface density defined by Eq. (6.5) and  $\Sigma_0$  the central surface mass density of the spiral galaxy (cf. Eq. (5.8)). In this case, the observer only sees one single image of the distant source. These properties will be better understood after reading section (6.1.5).



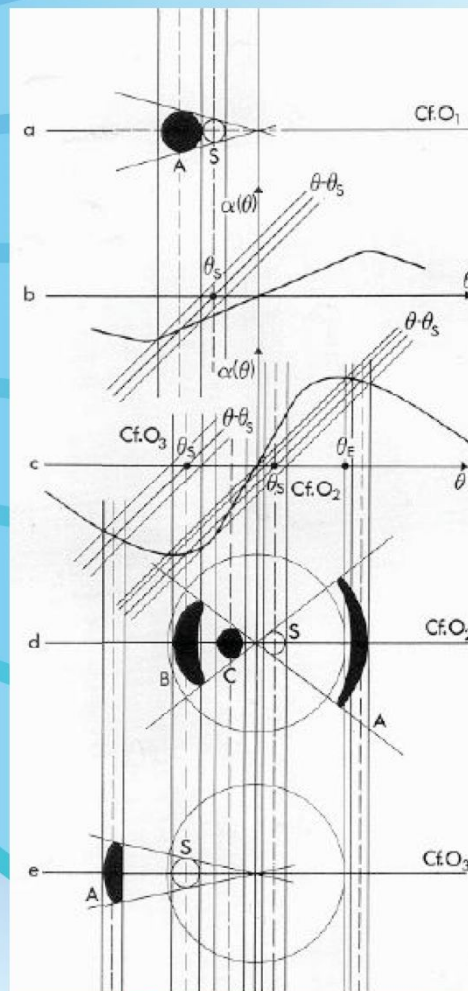
## 2. Gravitational lenses

### 6. GL MODELS:

#### 6.1. Axially symmetric lens models:

Combined bending angle diagrams (b and c) and resulting lensed images produced for the circular source S by a spiral galaxy lens model (a, d and e; see text).

Numerical simulations Caus2.exe and/or Caustics.exe !!!



### 2. Gravitational Lenses:

#### 6. GRAVITATIONAL LENS MODELS:

##### 6.1. Axially symmetric lens models:

##### 6.1.4. The spiral galaxy lens model:

However, when the observer is located behind the focal point ( $\Sigma_0 > \Sigma_c$ ), he may see either 3 images (cf.  $O_2$  in the corresponding figures) or one single image (cf.  $O_3$ ), depending on whether he is located within, or outside, the caustic line. This caustic is very well seen in the ray tracing diagram as the envelope curve formed by the deflected light rays, which are tangent by pairs, originating from a very distant point source. Mathematically, the caustic corresponds to the solution of Eq. (4.6) for the case when the magnification of one of the lensed images gets infinitely large (i.e.  $\mu_i \rightarrow \infty$ ). We will see in section 6.2. that caustics constitute generic features characterizing realistic lens models and that, very generally speaking, an observer crossing a caustic (cf. going from the positions  $O_2$  to  $O_3$ ) always sees two of the lensed images approaching each other, getting very bright while they merge, and then totally vanishing when the observer gets on the other side of the caustic. For the case of the spiral galaxy lens model, this sequence of events may easily be understood while changing the position of the source in the bending angle diagram illustrated above.

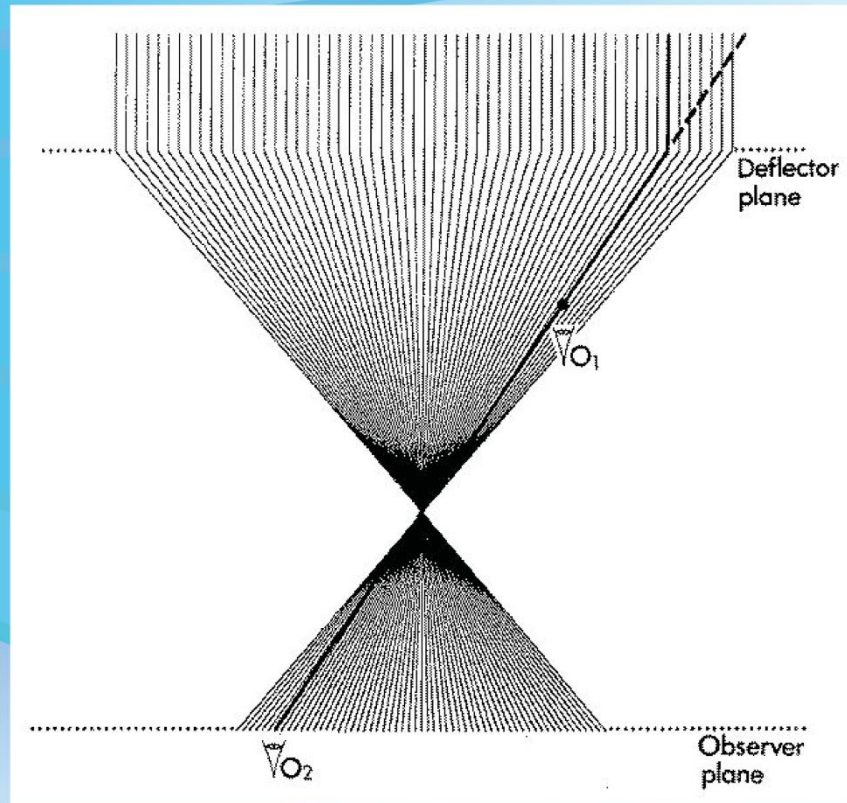
See also the numerical simulations Caus2.exe and/or Caustics.exe !!!

## 2. Gravitational lenses

### 6. GL MODELS:

#### 6.1. Axially symmetric lens models:

Ray tracing diagram for the uniform disk lens model.



### 2. Gravitational Lenses:

#### 6. GRAVITATIONAL LENS MODELS:

##### 6.1. Axially symmetric lens models:

##### 6.1.5. The uniform disk lens model:

A transparent circular disk of matter, seen face on, characterized by a uniform surface mass density  $\Sigma_0$  has an effective deflecting mass equal to  $\pi \xi^2 \Sigma_0$ , where  $\xi$  represents the impact parameter of a chosen light ray. The deflection angle is thus (see Eq. (4.5)) given by

$$\alpha(\xi) = 4\pi G \Sigma_0 \xi / c^2. \quad (6.29)$$

The disk is therefore acting as a normal converging lens (see the ray tracing diagram in the above figure), whose focal length is

$$f = \xi / \alpha(\xi) = c^2 / (4\pi G \Sigma_0). \quad (6.30)$$

Note that for a too small value of  $\Sigma_0$  the focal length  $f$  may turn out to be larger than the size of the Universe.

It is then easy to show that the lens equation (4.3) leads to the solution

$$\theta = \theta_s / (1 - \kappa), \quad (6.31)$$

where  $\kappa = \Sigma_0 / \Sigma_c$ ,  $\Sigma_c$  being the critical surface mass density defined in Eq. (6.5).

## 2. Gravitational lenses

### 6. GL MODELS:

#### 6.1. Axially symmetric lens models:

$$\underline{\alpha}(\xi) = 4\pi G \Sigma_0 \xi / c^2. \quad (6.29)$$

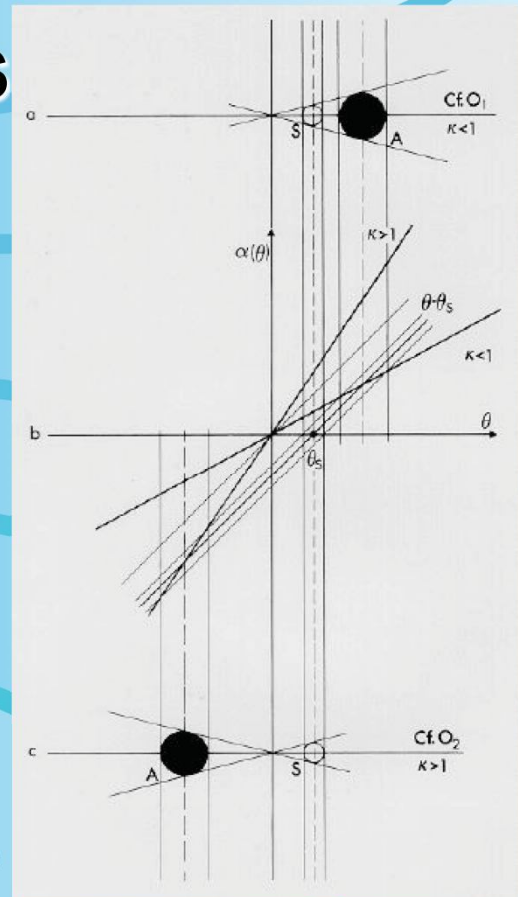
$$f = c^2 / (4\pi G \Sigma_0). \quad (6.30)$$

$$\theta = \theta_s / (1 - \kappa), \quad (6.31)$$

$$\kappa = \Sigma_0 / \Sigma_c,$$

$$\mu_A = 1 / (1 - \kappa)^2. \quad (6.32)$$

Combined bending angle diagram (b) and resulting lensed images produced for the circular source S by two different uniform disk lens models ( $\kappa < 1$  in (a) and  $\kappa > 1$  in (c); see text).



### 2. Gravitational Lenses:

#### 6. GRAVITATIONAL LENS MODELS:

##### 6.1. Axially symmetric lens models:

##### 6.1.5. The uniform disk lens model:

With the exception of a hypothetical observer that would be precisely located at the focal point ( $\kappa = 1$ , the perceived image would then be a fully illuminated disk of light!), the observer just sees one single image of the distant source, somewhat displaced and (de)magnified (see the combined bending angle diagram in the above figure). The magnification of the lensed image is directly found to be

$$\mu_A = 1 / (1 - \kappa)^2. \quad (6.32)$$

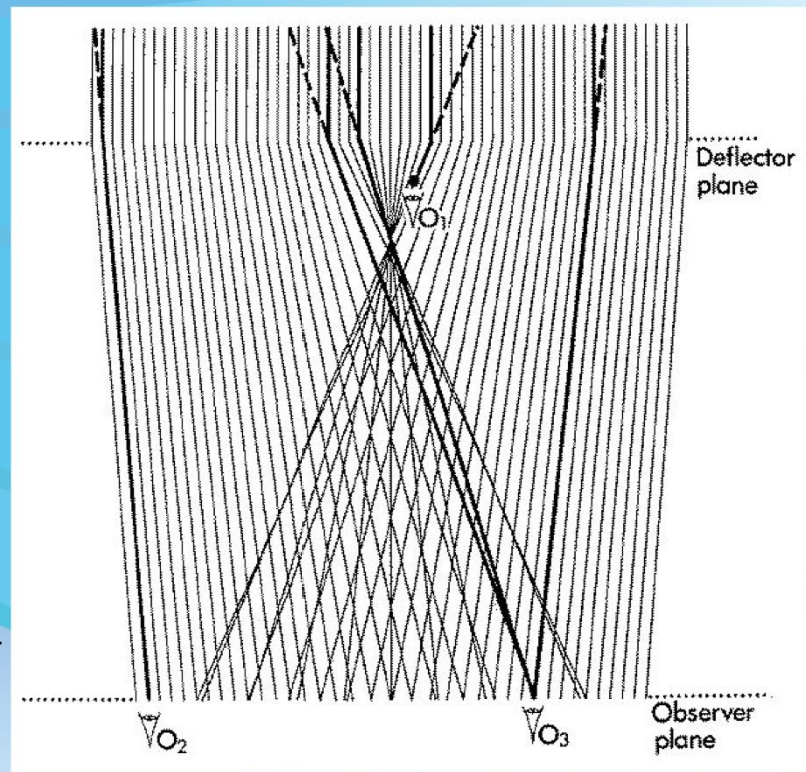
Let us note that for an observer located between the lens and the focal point we have  $\kappa < 1$  (cf.  $O_1$  in the corresponding figures), whereas we have  $\kappa > 1$  when the observer is located behind the focal point (cf.  $O_2$ ).

## 2. Gravitational lenses

### 6. GL MODELS:

#### 6.1. Axially symmetric lens models:

Ray tracing diagram for the truncated uniform disk lens model.



### 2. Gravitational Lenses:

#### 6. GRAVITATIONAL LENS MODELS:

##### 6.1. Axially symmetric lens models:

##### 6.1.6. The truncated uniform disk lens model:

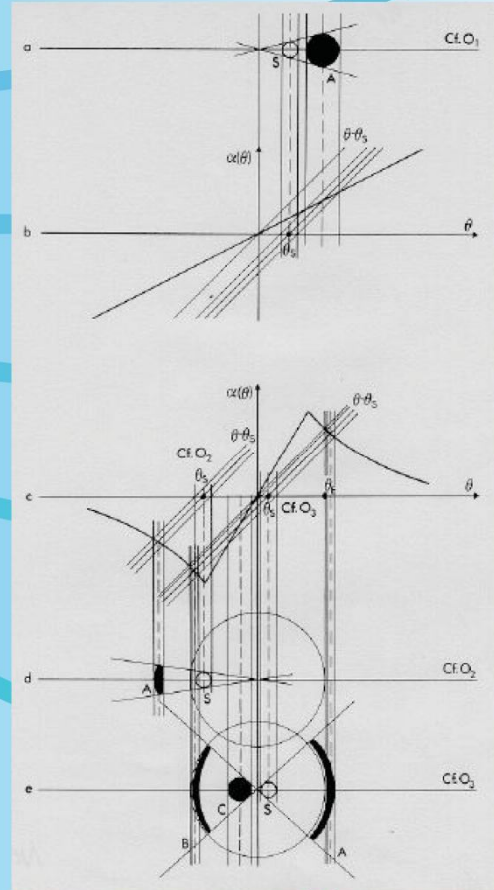
Let us finally consider the case of a truncated uniform disk, i.e. such that we may possibly have  $\xi > R$ . For those external rays, the disk effectively acts as a point mass and the lens equation leads to a combination of the solutions (6.9) and/or (6.31), depending on whether the condition  $\theta > R / D_{od}$  or  $\theta < R / D_{od}$  is fulfilled. From the ray tracing diagram depicted in the above figure and the combined bending angle diagrams represented on the next composite figure, we see that only one image can be formed for  $\kappa < 1$  (cf.  $O_1$  on the next figures), whereas for  $\kappa > 1$ , there may result the formation of one or three images (cf.  $O_2$  and  $O_3$ ).

## 2. Gravitational lenses

### 6. GL MODELS:

#### 6.1. Axially symmetric lens models:

Combined bending angle diagrams (b and c) and resulting lensed images produced for the circular source S by a truncated uniform disk lens model (a, d and e; see text).



### 2. Gravitational Lenses:

#### 6. GRAVITATIONAL LENS MODELS:

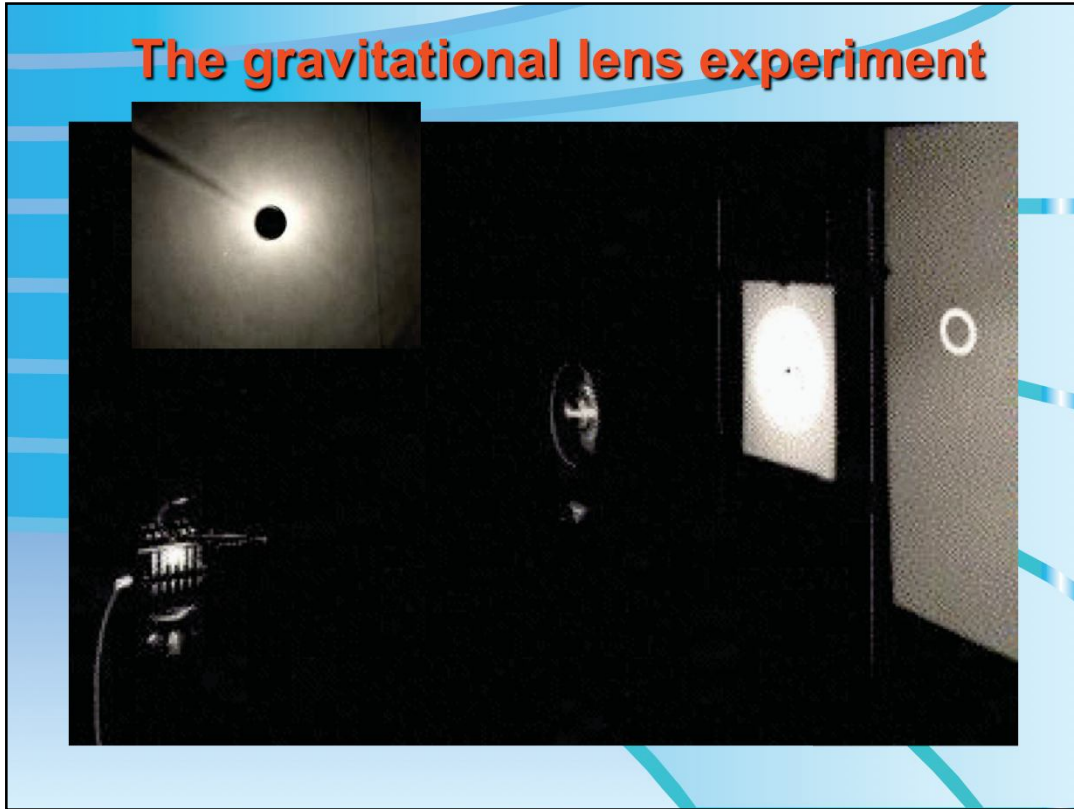
##### 6.1. Axially symmetric lens models:

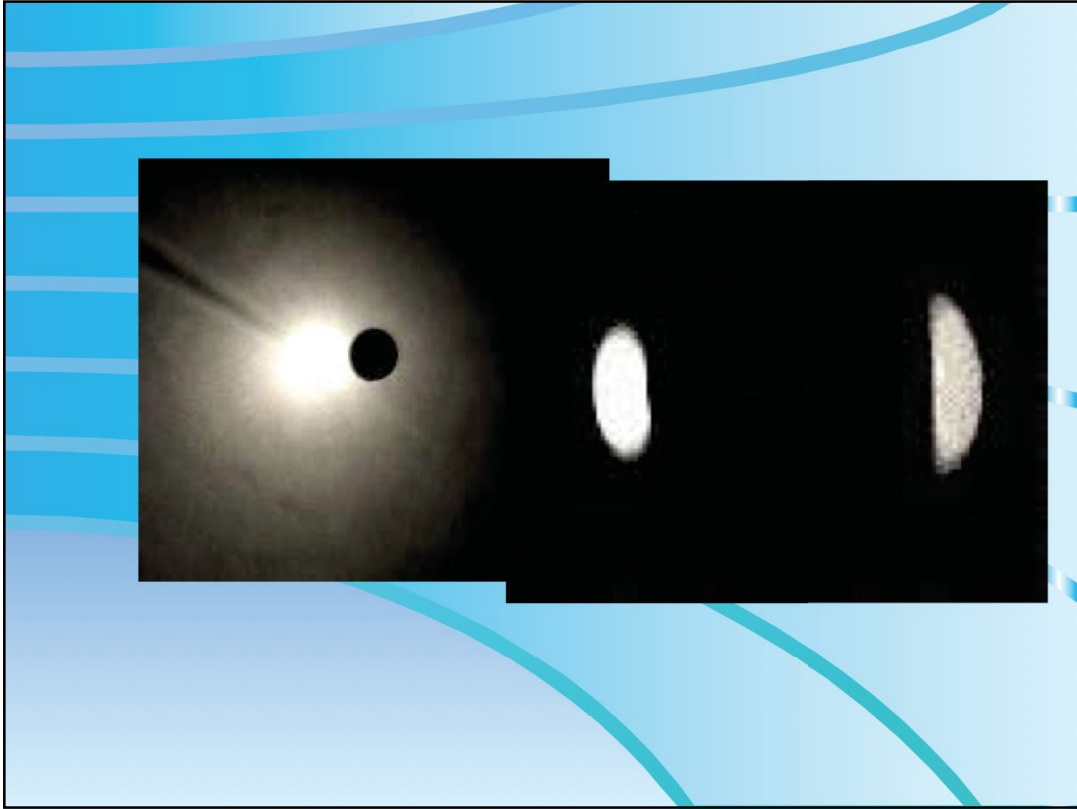
##### 6.1.5. The truncated uniform disk lens model:

Numerical simulations (<http://pcollette.webege.com/>)!!!

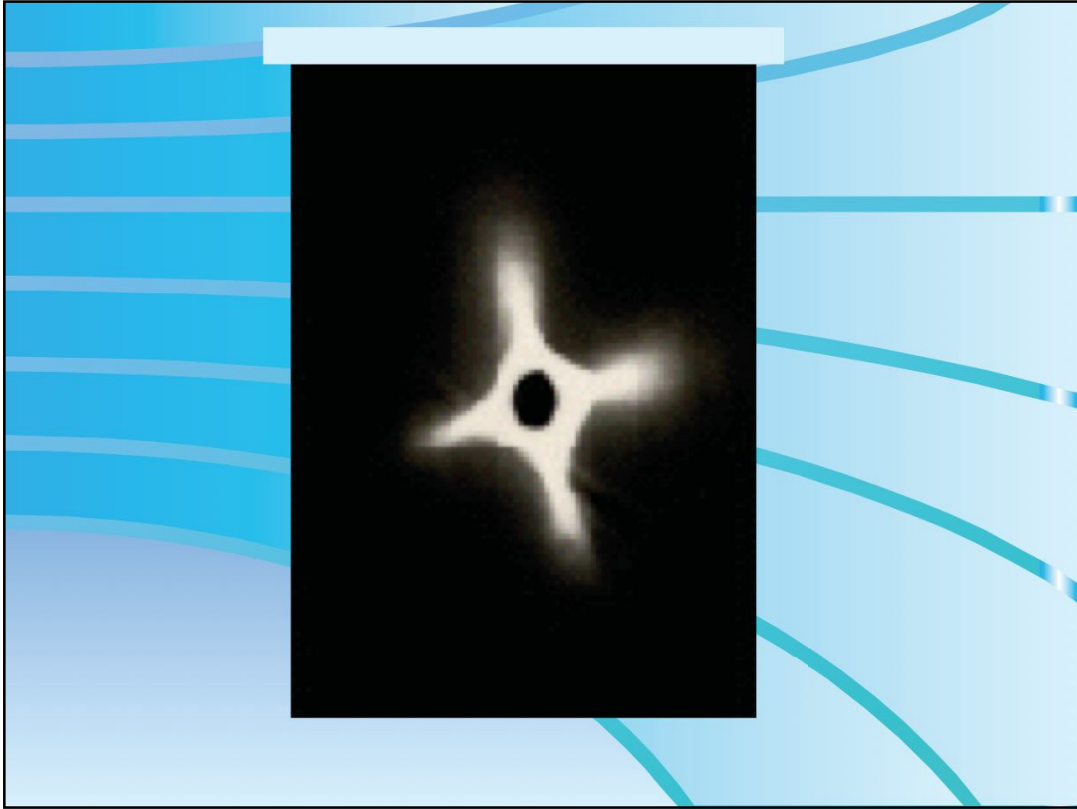
30/9/2011

13







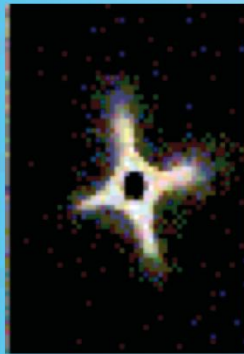


## 2. Gravitational lenses

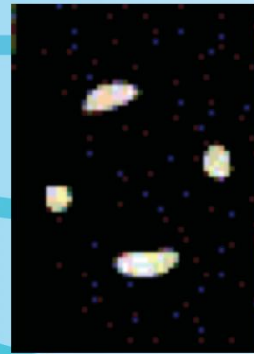
### 6. GL MODELS; 6.2. Asymmetric lenses:



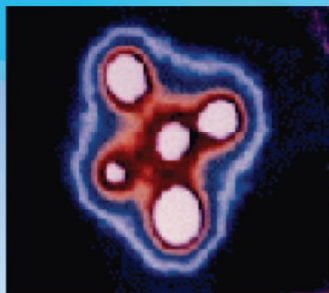
(z)



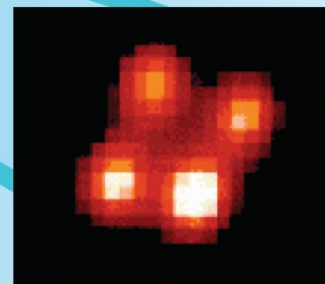
(a)



(b)



2237+0305,  $\Delta\theta \sim 1.5''$ ,  
 $z_q = 1.69$ ,  $z_d = 0.04$



H1414+117,  $\Delta\theta \sim 1''$ ,  
 $z_q = 2.55$ ,  $z_d = ?$

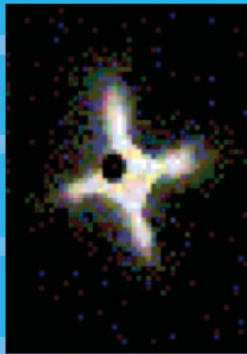
## 2. Gravitational Lenses: 6. GRAVITATIONAL LENS MODELS:

### 6.2. Asymmetric lenses:

Let us first summarize some of the important results that have been obtained in the previous section when considering the formation of multiple images by an axially symmetric lens model. For the case of the point mass and SIS deflectors that are singular in their center (i.e. the deflection angle is undefined or  $\rightarrow \infty$  as the impact parameter  $\rightarrow 0$ ), the maximum number of lensed images has been found to be equal to two. For non singular deflectors such as the spiral galaxy or the truncated uniform disk, we have seen that there were one or, at most, three lensed images, one of these being often very faint and located very near to the center of the lens. As we may expect, symmetric lenses are very seldomly realized in nature; usually the main lens itself is asymmetric or some asymmetric disturbances may also be induced by the presence of neighbouring masses. In an important paper, Burke (1981) has demonstrated that a non singular, transparent (symmetric or asymmetric) lens does always produce an odd number of images for a given point source (except when located on the caustics). However, for the case of a singular lens, as in our optical lens experiment, one may obtain an even number of images. In our optical gravitational lens experiment (cf. section 5.2.), the effects of a typical non symmetric (singular) gravitational lens may be simulated by simply tilting the optical lens. In this case (see the above figure a), the bright focal line along the optical axis which existed in the symmetric configuration (figure z) has changed into a two dimensional caustic surface, a section of which is seen as a diamond shaped caustic (made of four folds and four cusps) in the pinhole plane. As a result, the Einstein ring that was observed in the symmetric case has now split up into four lensed images (Fig. b). Similar observed examples of gravitational lenses are the multiply imaged quasars 2237+0305 (known as the Einstein Cross) and H1413+117 (the Clover-Leaf).

## 2. Gravitational lenses

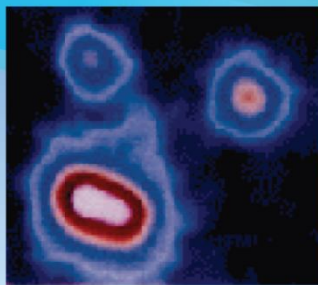
### 6. GL MODELS; 6.2. Asymmetric lenses:



(c)



(d)



PG1115+080,  $\Delta\theta \sim 2''$ ,  
 $z_q = 1.72$ ,  $z_d = 0.29$



0414+0534,  $\Delta\theta \sim 3''$ ,  
 $z_q = 2.63$ ,  $z_d = 0.96$

### 2. Gravitational Lenses:

#### 6. GRAVITATIONAL LENS MODELS:

##### 6.2. Asymmetric lenses:

Such a configuration of four lensed images always arises when the pinhole (observer) lies inside the diamond formed by the caustic. Let us immediately note that such caustics constitute a generic property of gravitational lensing, the focal line in the symmetric configuration (Fig. z) being just a degenerate case. Fig. d above shows the merging of two of the four images into one, single, bright image when the pinhole approaches one of the fold caustics (Fig. c). Some well known multiply imaged quasars showing similar image configurations are PG1115+080 (the triple quasar) and 0414+0534 (the dusty lens).

## 2. Gravitational lenses

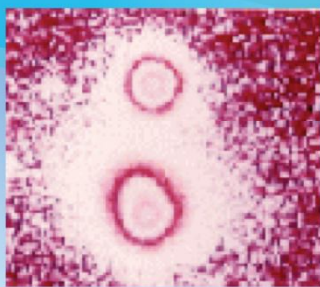
### 6. GL MODELS; 6.2. Asymmetric lenses:



(e)

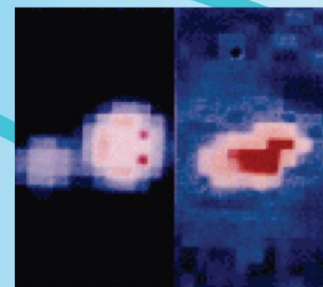


(f)



Q0957+561,  $\Delta\theta \sim 6''$ ,  
 $z_q = 1.41$ ,  $z_d = 0.36, 0.5$

Lensed  
Quasar



Lens

UM673,  $\Delta\theta \sim 2''$ ,  
 $z_q = 2.72$ ,  $z_d = 0.49$

### 2. Gravitational Lenses:

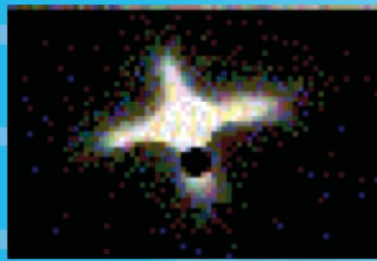
### 6. GRAVITATIONAL LENS MODELS:

#### 6.2. Asymmetric lenses:

Just after the pinhole has passed the fold caustic (see Fig. e), the two merging images have totally disappeared (Fig. f). Known doubly imaged quasars are Q0957+561 (the double quasar) and UM673.

## 2. Gravitational lenses

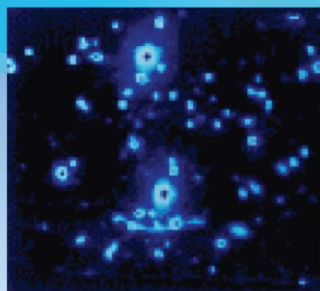
### 6. GL MODELS; 6.2. Asymmetric lenses:



(g)



(h)



Abell370,  $\Delta\theta \sim 20''$ ,  
 $z_s = 0.725$ ,  $z_d = 0.37$



Cl2244-02,  $\Delta\theta \sim 20''$ ,  
 $z_q = 2.237$ ,  $z_d = 0.34$

### 2. Gravitational Lenses:

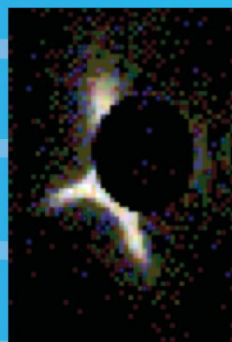
#### 6. GRAVITATIONAL LENS MODELS:

##### 6.2. Asymmetric lenses:

A particularly interesting case occurs when the pinhole (observer) is located very close to one of the cusps (cf. Fig. g). Three of the four previous images have then merged into one luminous arc, whereas the fourth one appears as a faint counterimage (Fig. h). Famous luminous arcs have been identified in the rich galaxy clusters Abell370 and Cl2244-02.

## 2. Gravitational lenses

### 6. GL MODELS; 6.2. Asymmetric lenses:



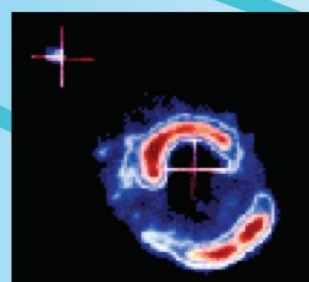
(i)



(j)



1131+0456,  $\Delta\theta \sim 2''$ ,  
 $z_s = 1.13?$ ,  $z_d = 0.85?$



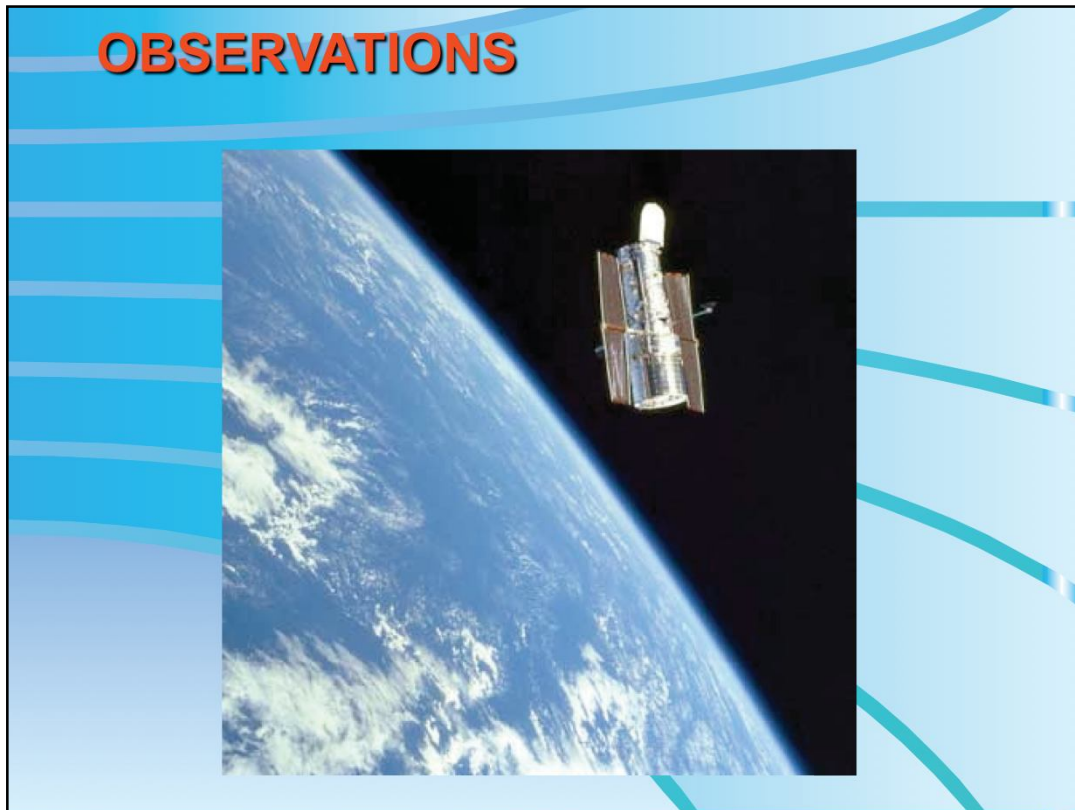
1654+1346,  $\Delta\theta \sim 2''$ ,  
 $z_s = 1.74$ ,  $z_d = 0.25$

### 2. Gravitational Lenses:

#### 6. GRAVITATIONAL LENS MODELS:

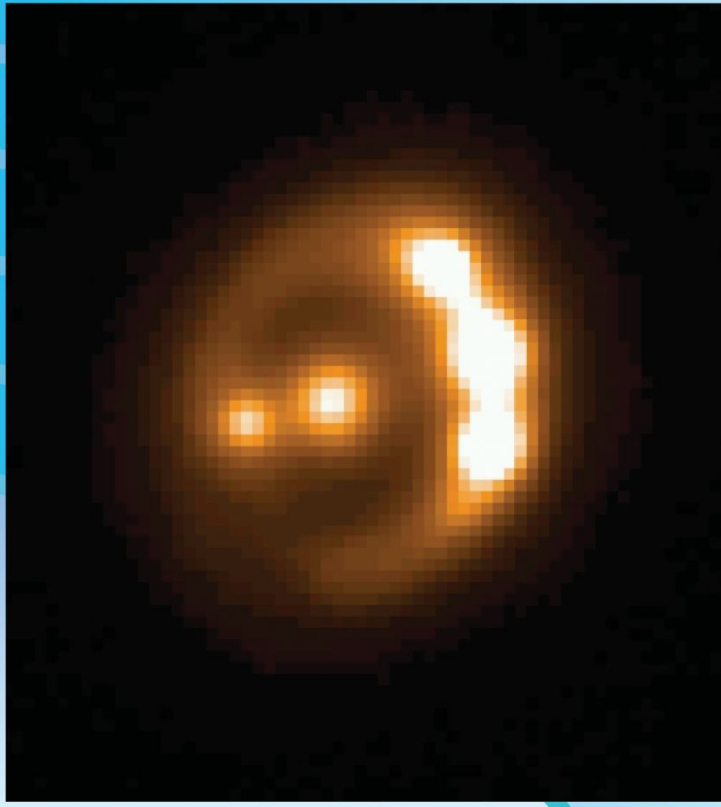
##### 6.2. Asymmetric lenses:

For large sources that cover most of the diamond shaped caustic (Fig. i), an almost complete Einstein ring is observed (Fig. j), although the source, lens and observer are not perfectly aligned and the lens is still being tilted. In this last experiment, the increase of the source size has been simulated by enlarging the pinhole radius by a factor  $\sim 4$ . In order to show that this is a correct simulation, one may consider the pinhole and the screen behind it as a camera. It is then clear that an increase in the size of the pinhole leads to a larger and less well focused image of the compact source, corresponding indeed to an increase in the source size. A more detailed and rigorous analysis does confirm this result. Several radio Einstein rings have been discovered among which 1131+0456 and 1654+1346.



## 2. Gravitational lenses

### 6. GL MODELS; 6.2. Asymmetric lenses:



#### 2. Gravitational Lenses:

#### 6. GRAVITATIONAL LENS MODELS:

#### 6.2. Asymmetric lenses:

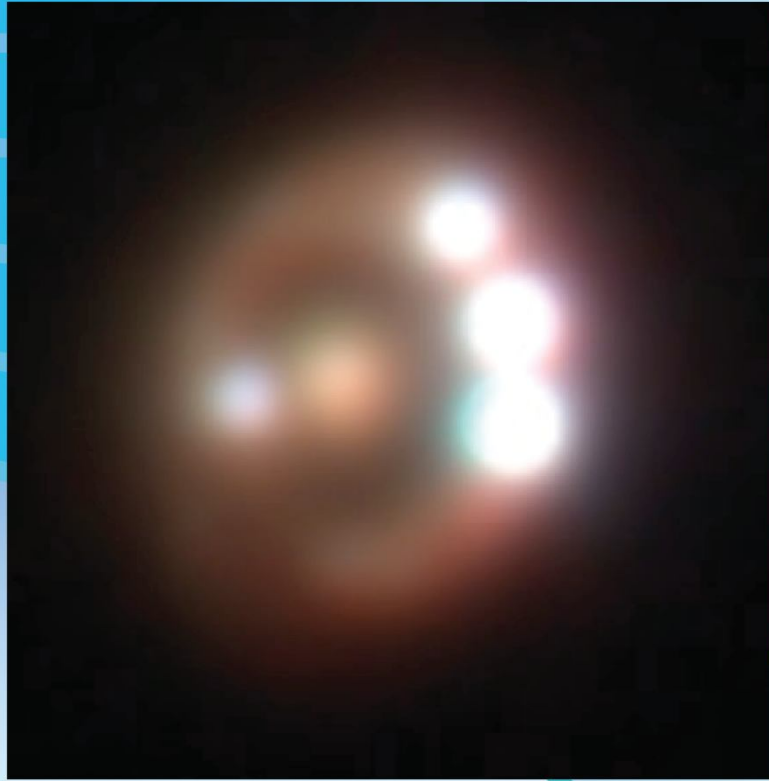
An optical Einstein ring altogether with a quadruply imaged quasar (RXS J1131-1231) has recently been discovered by the Liège group and is shown on the above slide (Sluse et al. 2003).

Arclets + optical simulation with mask!



## 2. Gravitational lenses

### 6. GL MODELS; 6.2. Asymmetric lenses:



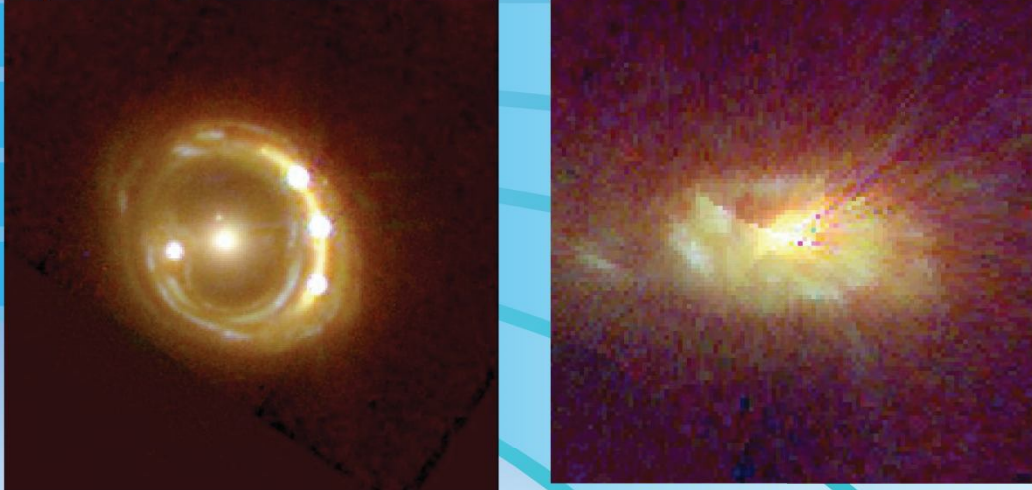
#### 2. Gravitational Lenses:

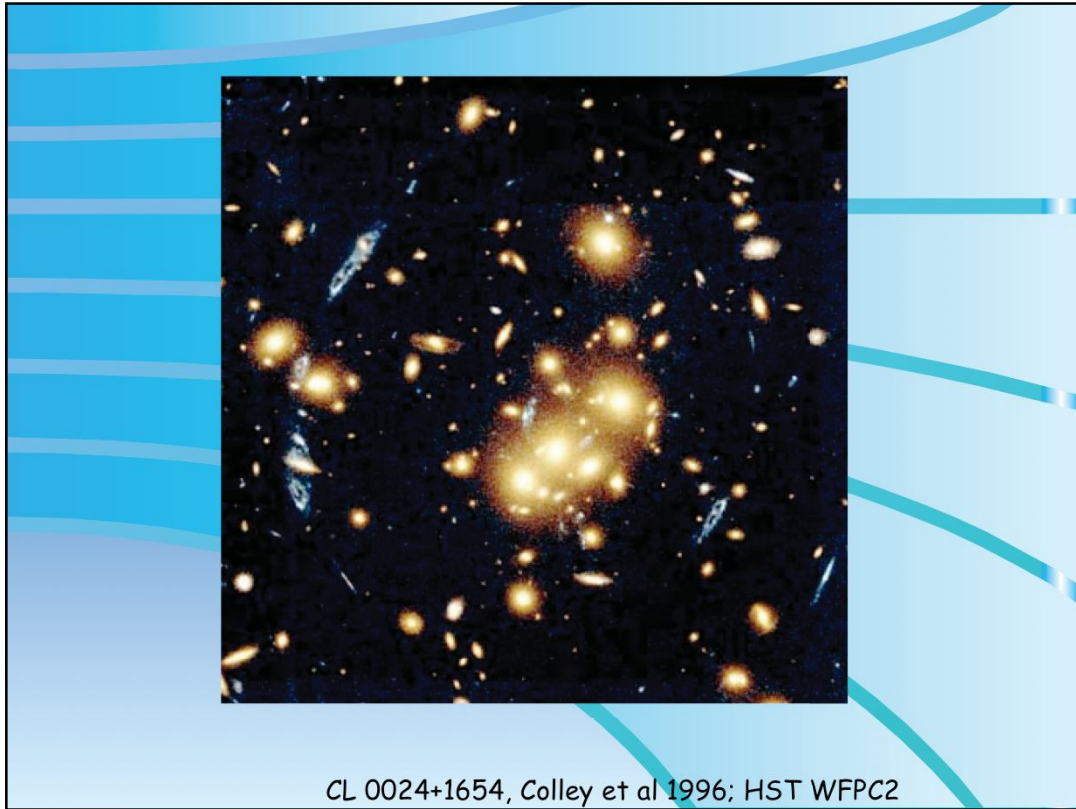
#### 6. GRAVITATIONAL LENS MODELS:

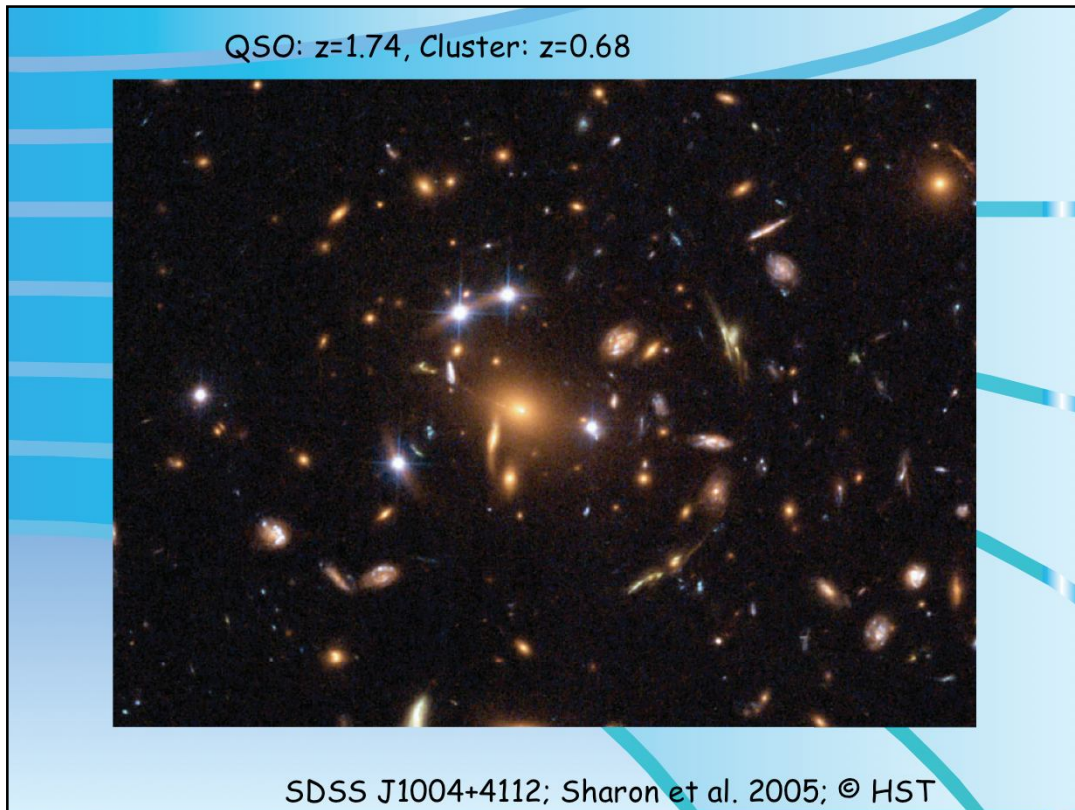
#### 6.2. Asymmetric lenses:

Composite color picture of RXS J1131-1231 (Sluse et al. 2003).

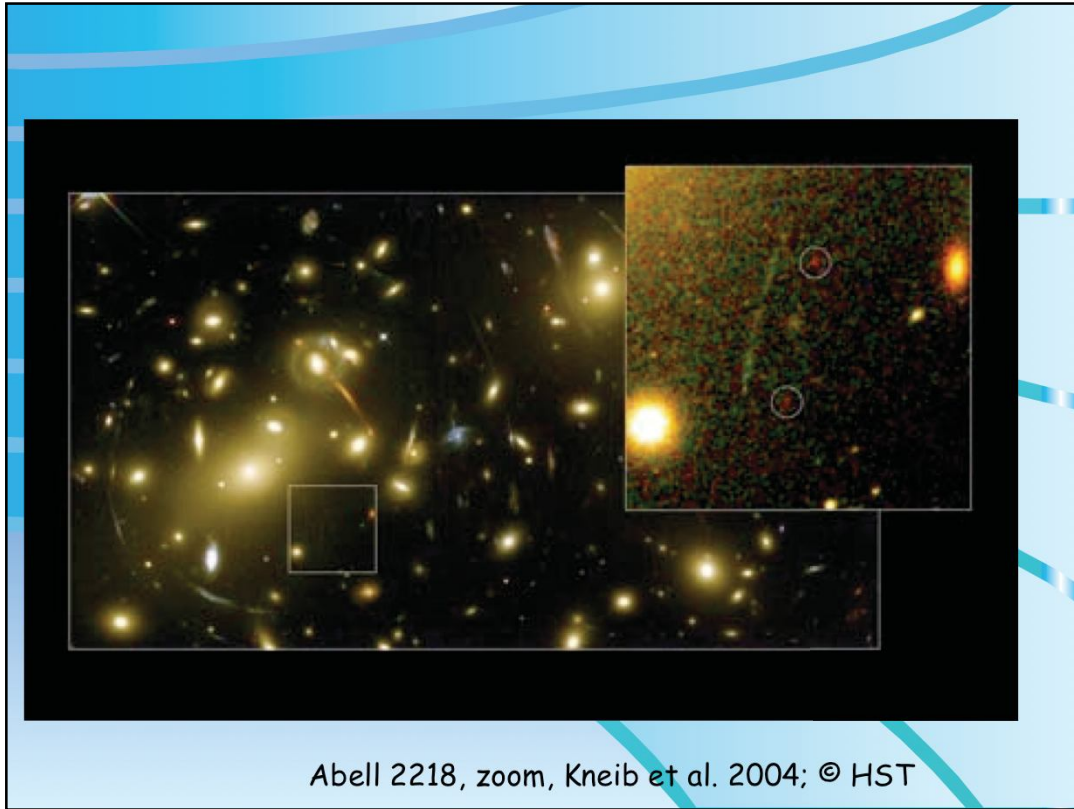
***RXS J11331-1231*** (Sluse et al. 2003, 2005, Claeskens et al. 2006) :  $z_s=0.658$ ,  $z_l=0.295$

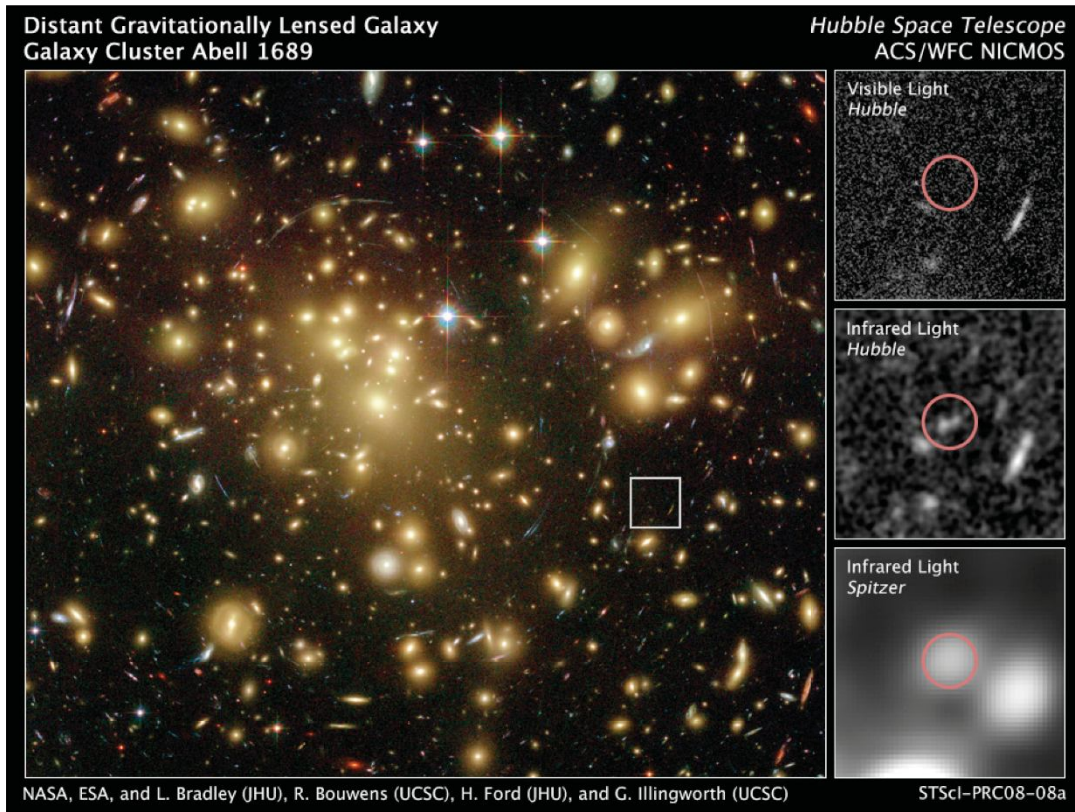


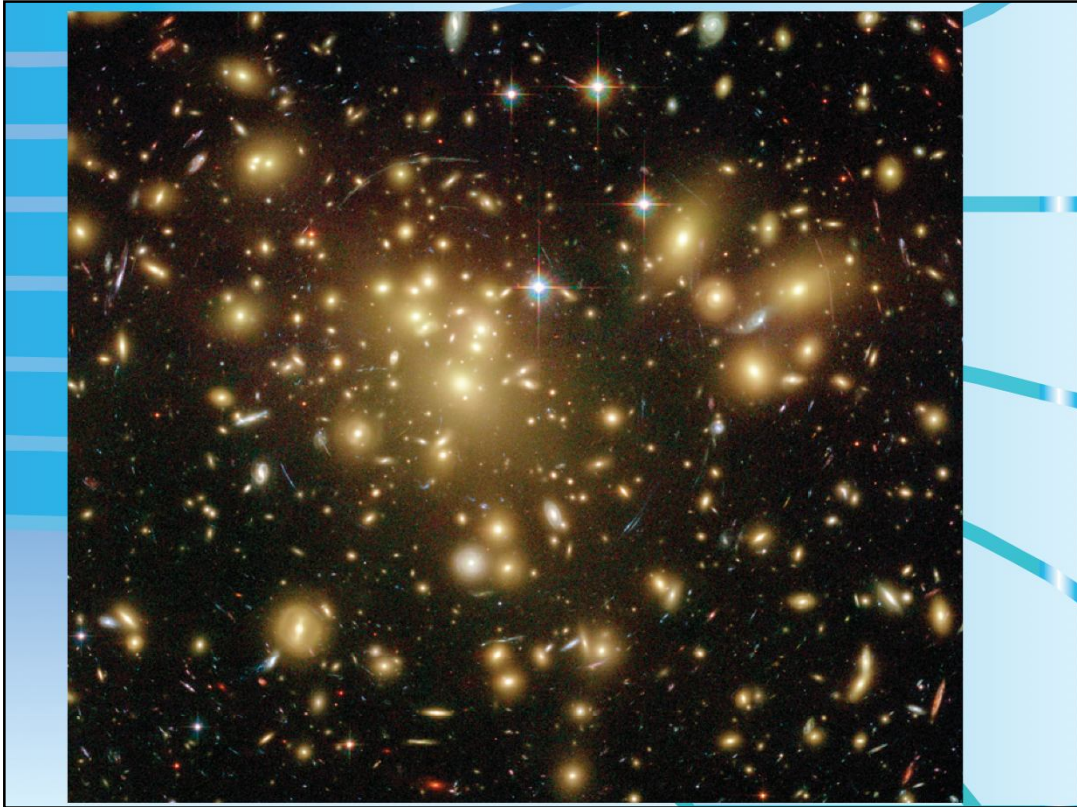








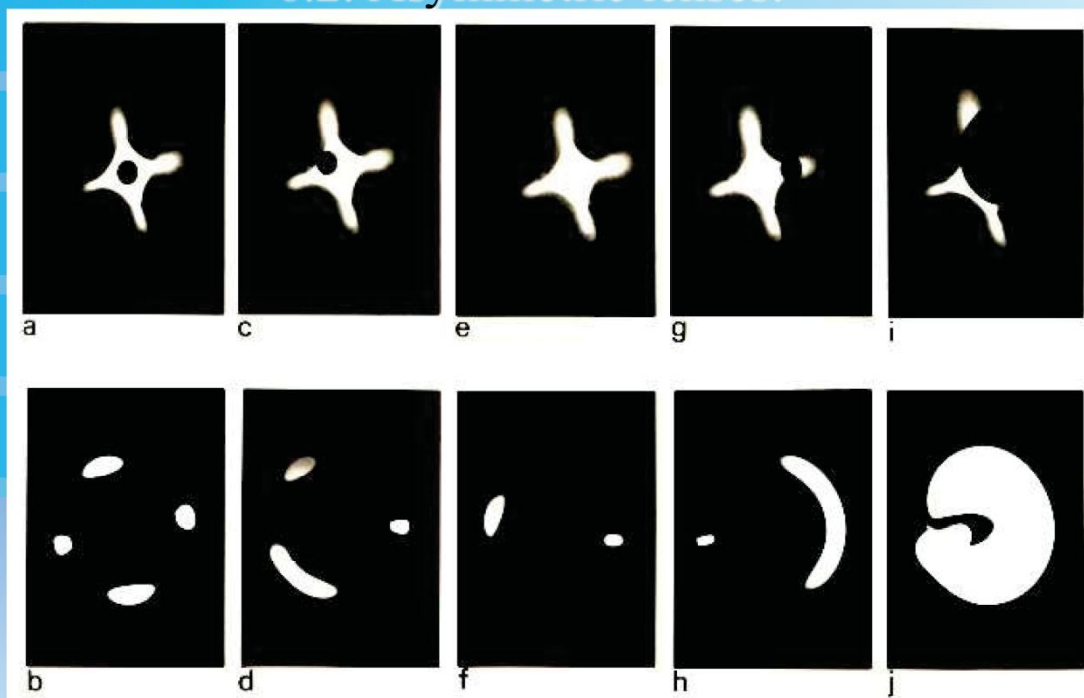






## 2. Gravitational lenses

### 6. GL MODELS: 6.2. Asymmetric lenses:



The optical gravitational lens experiment for the case of an asymmetric, singular deflector (see text in section 6.2.).

### 2. Gravitational Lenses:

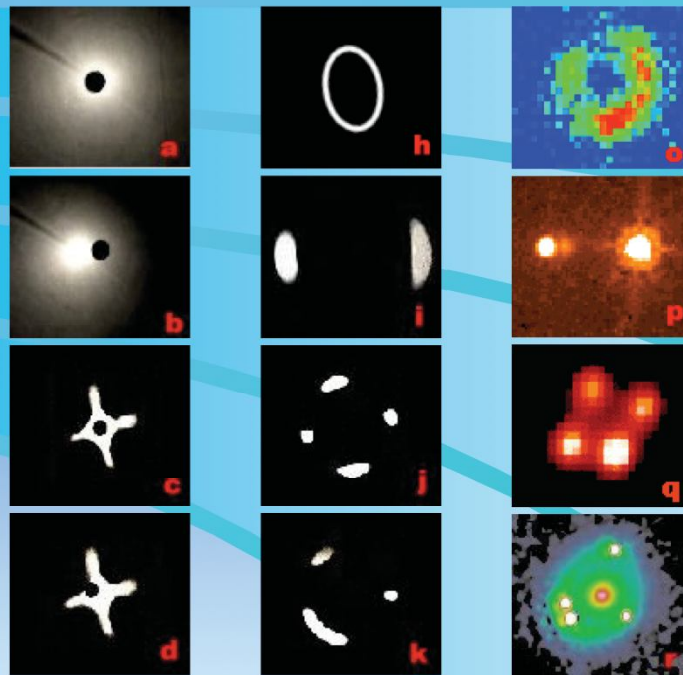
### 6. GRAVITATIONAL LENS MODELS:

#### 6.2. Asymmetric lenses:

The above figure summarizes all previous lensed image configurations reproduced by means of our gravitational lens simulator. As previously stated, the image configurations illustrated in Figs. a-j are all found among the observed gravitational lens systems. It is of course obvious that if our optical lens would have been constructed non-singular in the center (cf. the 'spiral galaxy' optical lens shown before), we would have seen an additional image formed in the central part of the lens. For the known lenses with an even number of observed images, it may well be that a black hole resides in the center of the lens. The presence of a compact core could also account for the "missing" image since then the very faint image expected to be seen close to, or through the core, would be well below the detection limits that are presently achievable. Let us finally note that whereas the formation of multiple lensed images by asymmetric gravitational lenses is mathematically well understood (cf. the pioneering work by Bourassa et al. 1973), the theoretical developments turn out to be very technical and rather tedious. The main results reduce however to the conclusions obtained in the above optical gravitational lens experiment.

## 2. Gravitational lenses

### 6. GL MODELS: 6.2. Asymmetric lenses:



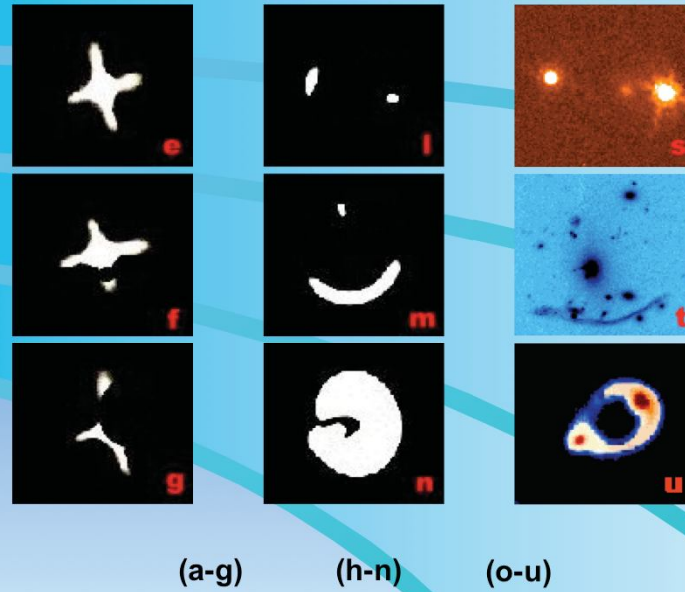
### 2. Gravitational Lenses:

### 6. GRAVITATIONAL LENS MODELS:

### 6.2. Asymmetrical lenses:

## 2. Gravitational lenses

### 6. GL MODELS: 6.2. Asymmetric lenses:



### 2. Gravitational Lenses:

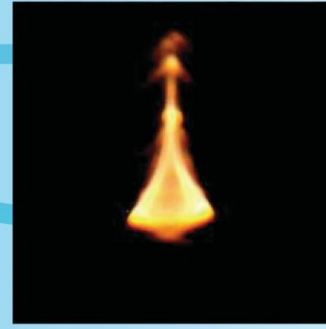
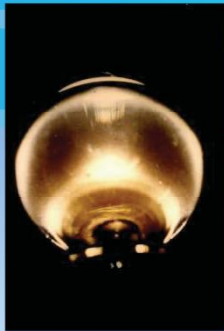
### 6. GRAVITATIONAL LENS MODELS:

### 6.2. Asymmetrical lenses:

## 2. Gravitational lenses

### 6. GL MODELS: 6.2. Asymmetric lenses:

Numerical  
simulations  
Mirage.exe !!!



Home made caustics using a glass with red wine (to minimize the chromatic effects) ... and the resulting multiple lensed images of a background source!

### 2. Gravitational Lenses:

### 6. GRAVITATIONAL LENS MODELS:

#### 6.2. Asymmetric lenses:

The above figures illustrate home made caustics using a glass with red wine (to minimize the chromatic effects) ... and the resulting multiple lensed images of a background source!

See also the numerical simulations with Mirage.exe ( $\eta = 0.5$ ,  $\varepsilon = -1.0, 0.0, 0.5$  using the double jet ... and 0.1 with pictures).

LATER: sharks and whales, funny house at the fair, swimming pool with coins, sun, etc.

# I. Didactical experiments

## Gravitational lensing:

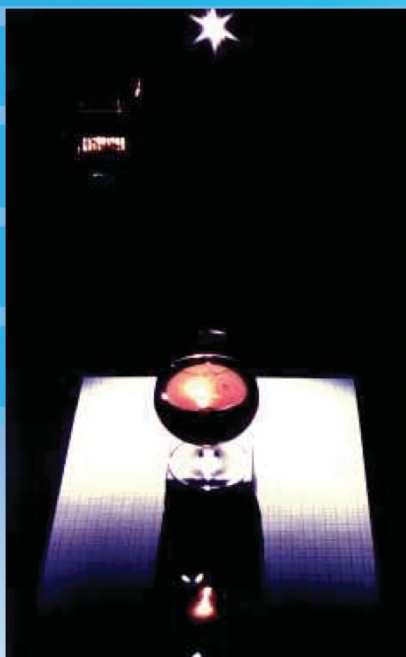


Figure 1: The wine glass experiment. A bright compact light source (upper image) is used as a distant quasar. The wine glass set on the table (cf. Figure 2) distorts the light rays from the quasar and produces a caustics having a triangular shape (see the enlargement in Figure 3). In order to see the multiple images from the distant quasar, put the glass at the very edge of the table and one of your eyes around the caustics (see text).

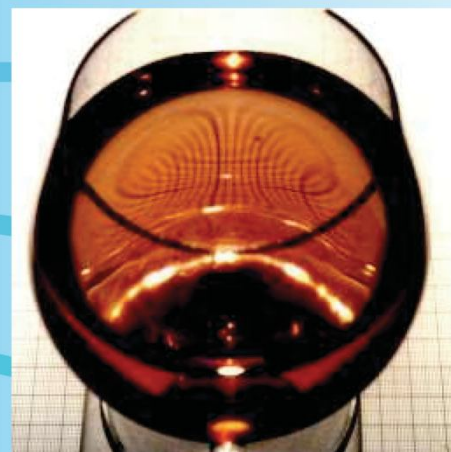


Figure 2: When looking through the wine glass, the distortion of the background field (millimetric paper) by the lens is very conspicuous.

### **6.2.1. Other examples of caustics and multiple imaging**

#### **6.2.1.1. Gravitational lensing and the wine glass experiment:**

The formation of multiple images of a distant quasar by the gravitational lensing effects of a foreground galaxy may be very simply, and faithfully, accounted for by the wine glass experiment described below.

In order to successfully make this experiment, please use as the quasar light source a candle, or a bright compact light source as shown in Figure 1. This light source is set at a typical distance of several meters from, and somewhat higher than, the table on which a glass full of wine is placed. Like a gravitational lens, the wine glass distorts the uniformly emitted light from the source. The nature of this distortion is very well seen in Figure 2. Back in the case depicted in Figure 1, we see that in front of the wine glass, the distribution of light on the table is no longer uniform: higher concentrations of light may be seen at some locations in the form of a caustics (i.e. the intersection of a three-dimensional caustics with the plane of the table). The latter is, in the present case, approximately triangular. The three sides and summits of this triangular caustics are named folds and cusps, respectively.

# I. Didactical experiments

## Gravitational lensing:

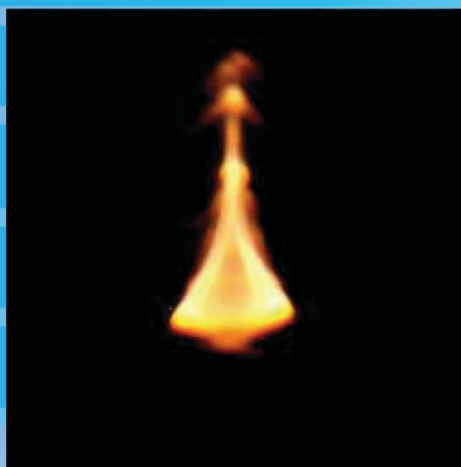


Figure 3: Enlargement of the triangular caustics visible in Figure 1. The caustics result from the redistribution of light rays emitted from the quasar by the wine glass.

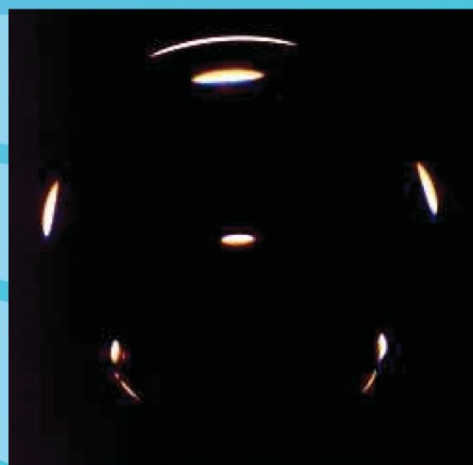


Figure 4: Multiple images of the compact light source seen by the objective of a photographic camera placed inside the caustics.

### **6.2.1. Other examples of caustics and multiple imaging**

#### **6.2.1.1 Gravitational lensing and the wine glass experiment:**

A blow up of this caustics is shown in Figure 3. The folds result from the envelope of pairs of tangent light rays from the candle. As a result, an observer setting his eye on a fold will see a pair of merging images from the distant quasar. Three merging images will be seen at the location of a cusp. In order to be able to put your eye at various locations with respect to the caustics, it is recommended to put the glass at the very edge of the table. You may then also observe that the total number of images increases by two when your eye crosses a fold from outside to inside the caustics. Figure 4 shows a photograph made with a camera set up at the center of the caustics. Up to 9 different images of the compact light source are visible.

As an exercise, draw various diagrams showing the multiple image configurations of the background light source for different positions of your eye with respect to the caustics (folds and cusps) and compare them with the multiple image configurations observed for the known cases of multiply imaged quasars (a gallery of pictures illustrating various cases of multiply imaged quasars is available via the URL: [http://vela.astro.ulg.ac.be/grav\\_lens/](http://vela.astro.ulg.ac.be/grav_lens/)).

Note that the formation of caustics of light is a very generic feature in nature. It arises whenever a foreground object (cf. the wine glass in the above experiment, a galaxy acting as a gravitational lens, the wavy interface between air and water in a swimming pool, on a lake, etc.) distorts the propagation of light rays from a distant light source. For instance, for each quasar-galaxy pair considered in the Universe, a more or less complex three dimensional caustics is formed behind each galaxy. Whenever an observer lies close to such a caustics, the former sees multiple images of the distant quasar. Due to the relative

# I. Didactical experiments

## Gravitational lensing:

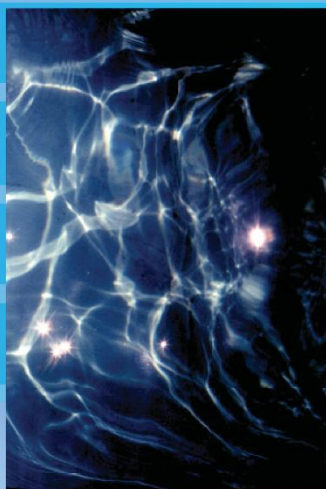


Figure 5: Caustics of light projected at the bottom of a swimming pool. The sun acts in this case as the distant light source.

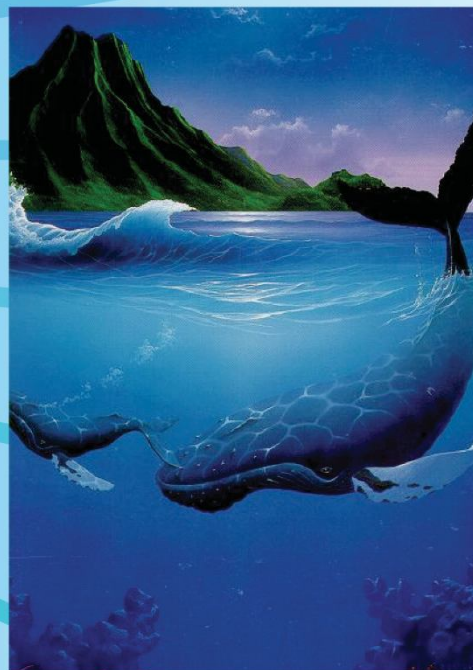


Figure 6: Caustics of light projected on the body of a whale, as painted by Miller. The moon light acts as the distant light source.

### **6.2.1. Other examples of caustics and multiple imaging**

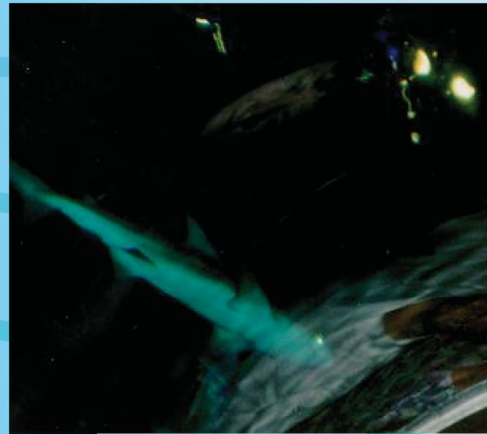
motion between the quasar, the lensing galaxy and the observer, this phenomenon does not last for ever. It can be shown that the typical lifetime of a cosmic mirage involving a quasar and a lensing galaxy is of the order of 20 million years.

#### **6.2.1.2 Multiple imaging as seen by whales and sharks:**

As already stated in the previous section, because of the wind, the interface between the air and the water in a swimming pool, on a lake, on a sea, etc., is wavy and as a result, the propagation of light rays from a distant source (cf. the sun, the moon, etc.) gets distorted when entering water. Here also, complex caustics are formed and Figure 5 reproduces a view of such caustics projected at the bottom of a swimming pool. Figure 6 illustrates also very well the caustics projected on the body of a whale, as drawn by the famous painter Miller.

# I. Didactical experiments

## Gravitational lensing:



Figures 7-9: Multiple images of external lights seen by sharks in the large pool at Sea World (Orlando, Florida).

### **6.2.1. Other examples of caustics and multiple imaging**

#### **6.2.1.2 Multiple imaging as seen by whales and sharks:**

There is consequently no doubt that, whenever one of the eyes of a whale crosses the folds (resp. the cups) of the complex caustics, the sun, the moon ... appear to them in the form of, continuously changing, multiple images, arcs, etc. Such multiple images, seen by real sharks inside the large pool at Sea World (Orlando), have been photographed by one of us in February 1994 and are reproduced in Figures 7-9.



# I. Didactical experiments

**Gravi-  
tational  
lensing:**



Figure 10: Reflected caustics and distorted (elongated, multiple, ...) images of coins placed at the bottom of a swimming pool.

## **6.2.1. Other examples of caustics and multiple imaging**

### **6.2.1.3 Multiple imaging in a swimming pool:**

Wonderful reflected caustics and distorted (multiply imaged, elongated, ...) images of coins placed at the bottom of a swimming pool (courtesy of J. Schramm). These distortions are reminiscent of those of lensed galaxies located behind a massive foreground galaxy cluster.

# I. Didactical experiments:

## Gravitational lensing

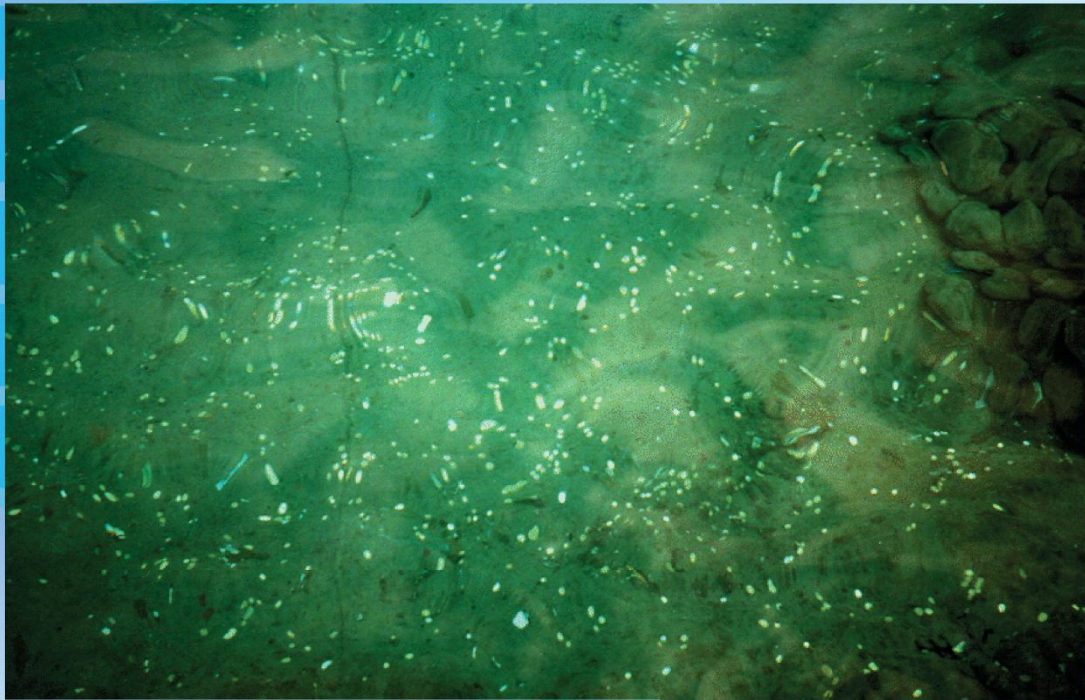


Figure 11: Distorted images of coins placed at the bottom of a swimming pool.

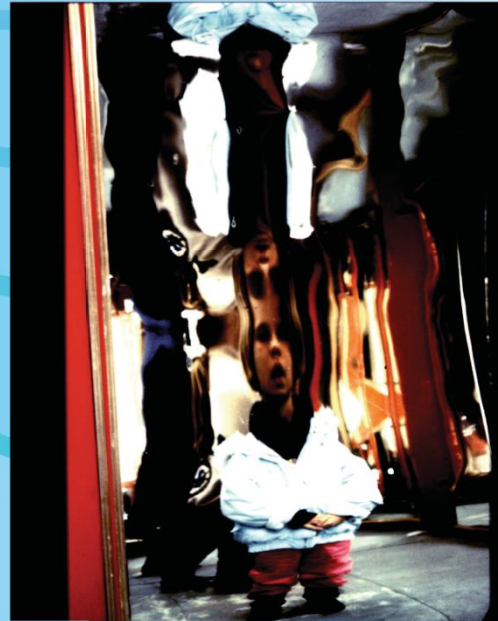
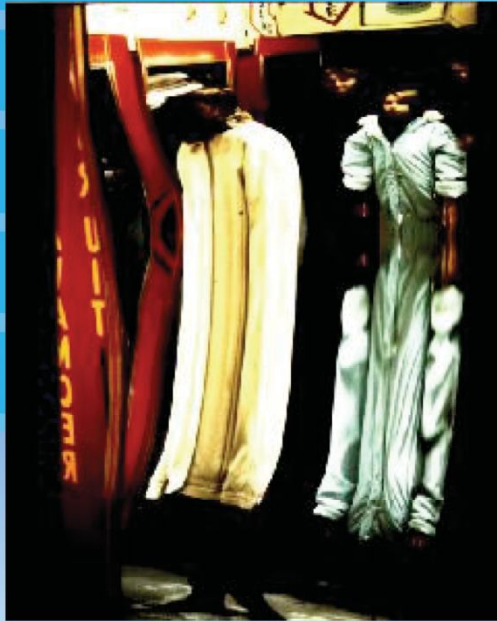
### **6.2.1. Other examples of caustics and multiple imaging**

#### **6.2.1.3 Multiple imaging in a swimming pool:**

Nicely distorted images of coins placed at the bottom of a swimming pool are very conspicuous in Fig. 11 (courtesy of J. Schramm). These distorted images are reminiscent of those of lensed galaxies located behind a massive foreground galaxy cluster.

# I. Didactical experiments

## Gravitational lensing:

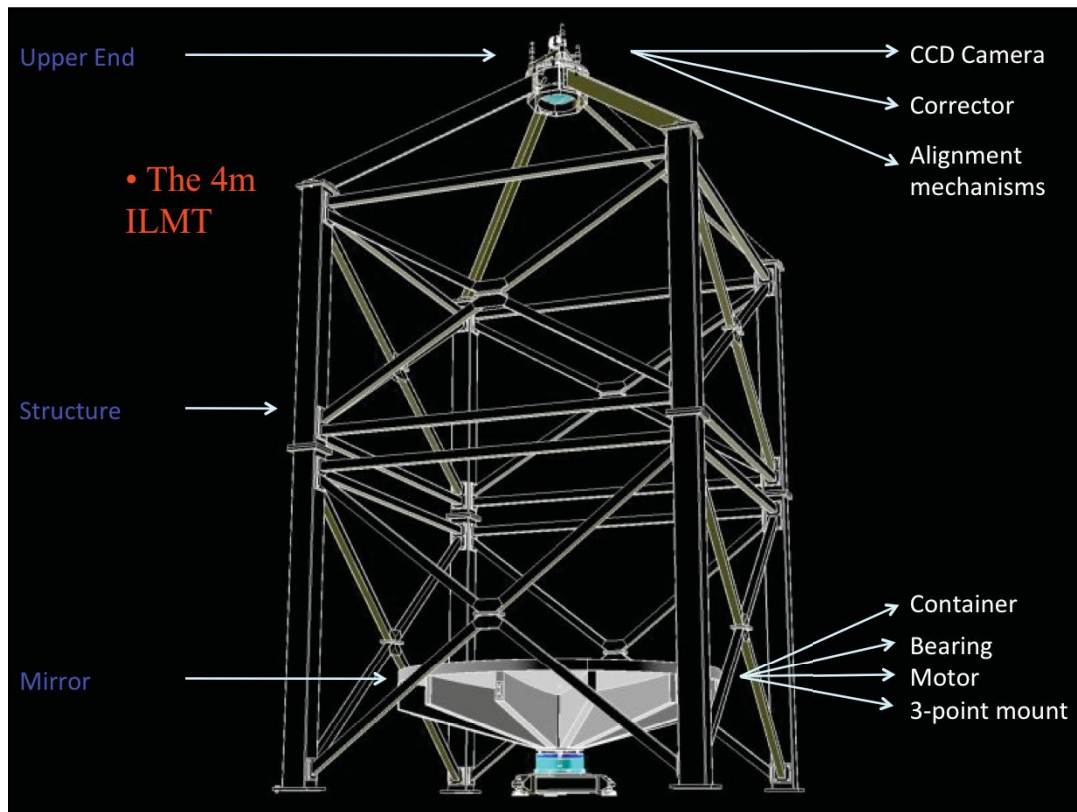


Figures 12 and 13: Multiple images of Virginie and Isabelle photographed at the House of Mirrors during the Liège october fair in 1989.

### **6.2.1. Other examples of caustics and multiple imaging**

#### **6.2.1.4 Multiple imaging at the fair house:**

Finally, one may also observe funny multiple images of human beings at the fair house. These are produced by wavy mirrors that distort the light rays emerging from the visitors. Several pictures taken at the Liège october fair in 1989 are shown in Figures 12-13.



## The International 4m LMT project



## The International 4m LMT project



## The International 4m LMT project



